

Teleportation using coupled oscillator states

P.T. Cochrane, G.J. Milburn and W.J. Munro

Department of Physics, The University of Queensland, QLD 4072, Australia.

(February 5, 2020)

We analyse the variation of teleportation fidelity with resource entanglement for three entanglement resources: two mode harmonic oscillator states with fixed total photon number, beam splitter generated harmonic oscillator states with fixed total photon number and the two-mode squeezed vacuum state. We define corresponding teleportation protocols for each example. The variation of entanglement in each case is modelled using phase noise.

I. INTRODUCTION

Quantum entanglement plays a central role in the emerging fields of quantum computation [1–5], quantum cryptography [6,7], quantum teleportation [8–13], superdense coding [14] and quantum communication [15–17]. The characterisation of entanglement is a challenging problem [18–23] and considerable effort has been invested in characterising entanglement in a variety of contexts [24–30].

One such context, quantum teleportation, has played a crucial role in understanding how entanglement can be used as a resource for communication. The recent experimental demonstrations [31,32] suggest that quantum teleportation could be viewed as an achievable experimental technique to quantitatively investigate quantum entanglement. Teleportation is a way of transmitting an unknown quantum state to a distant receiver with far better reliability than can be achieved classically. As the entanglement of the enabling resource is degraded, the fidelity of the teleportation protocol is diminished.

In this paper we attempt to make this intuition more precise using specific examples from quantum optics. Three entangled resources are considered: two mode harmonic oscillator states with fixed total photon number, beam splitter generated harmonic oscillator states with fixed total photon number and the two-mode squeezed vacuum state [33]. The examples we discuss exhibit quantum correlations between the photon number in each mode and, simultaneously, between the phase of each mode. To degrade the entanglement of the resource we consider phase fluctuations on each mode independently. In the limit of completely random phase we are left with only the classical intensity (photon number) correlations. The ability of the resources to teleport a state is shown to improve with the energy available in the resource, and therefore the dimension of the Fock space.

II. ENTANGLEMENT AND TELEPORTATION

Intuitively entanglement refers to correlations between distinct subsystems that cannot be achieved in a clas-

sical statistical model. Of course correlations can exist in classical mechanics, but entanglement refers to a distinctly different kind of correlation at the level of quantum probability amplitudes. The essential difference between quantum and classical correlations can be described in terms of the separability of states [34–40,46]. A density operator of two subsystems is separable if it can be written as the convex sum [40]

$$\rho = \sum_A w^A \rho'_A \otimes \rho''_A \quad (1)$$

As an example we consider the density operator for two harmonic oscillators (a and b) which have correlated energy

$$\rho_{ab} = \sum_{n=0}^{\infty} p_n |n, n\rangle \langle n, n| \quad (2)$$

where we use the notation $|n, n\rangle = |n\rangle_a \otimes |n\rangle_b$. Such a state has perfectly correlated excitation energy in each mode, a classical correlation, but no entanglement. On the other hand the pure state

$$|\Psi\rangle_{ab} = \sum_{n=0}^{\infty} \sqrt{p_n} |n, n\rangle \quad (3)$$

has the same classical correlation but is not separable. In this form we see that it is possible for a separable and an entangled state to share similar classical correlations for some variables. Any state that is not separable is entangled, but it may be difficult to distinguish a separable state from an entangled state. Teleportation however will enable such states to be distinguished.

Consider a communication protocol in which the results of measurements made on a physical system are transmitted to a distant receiver. The goal of the receiver is to reconstruct the physical state of the source, using only local resources, conditioned on the received information. The communication that takes place is of course entirely classical. In a teleportation protocol there is one additional feature: quantum correlations, entanglement, are first shared between the sending and receiving station. The degree of entanglement shared by sender and

receiver is called the teleportation *resource*. If there is no shared quantum correlation between the sender and receiver, the protocol is called classical. The extent and nature of the quantum correlations in the resource determine the fidelity of the protocol. Under ideal conditions the unknown state of some physical system at the transmitting end can be perfectly recreated in another physical system at the receiving end. If there is no shared entanglement resource this is impossible. There are many ways in which actual performance can differ from the ideal. In this paper we analyse the change in performance of teleportation protocols as the entanglement resource is varied. Our primary objective is to use the fidelity of a teleportation protocol to compare and contrast different kinds of entangled oscillator states.

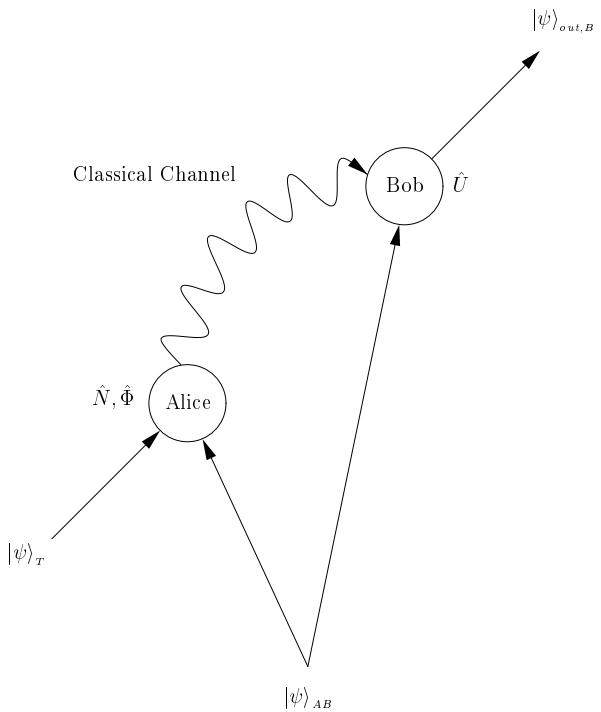


FIG. 1. General teleportation protocol. The entanglement resource $|\psi\rangle_{AB}$ and the classical channel are used to recreate the quantum state $|\psi\rangle_T$ at $|\psi\rangle_{out,B}$.

In general, teleportation proceeds as follows: the sender, Alice, has a *target* state, $|\psi\rangle_T$, she wishes to teleport to Bob, the receiver (see Figure 1). Alice and Bob each have access to one part of an entangled bipartite physical system prepared in the state $|\psi\rangle_{AB}$. In this paper the bipartite physical system is a two-mode electromagnetic field. In order to send the state of the target to Bob, Alice performs a joint measurement of number sum (\hat{N}) and phase difference ($\hat{\Phi}$) on the target and her mode. She then sends the information gained from these measurements to Bob via a classical channel. Bob performs local unitary transformations on the mode in his possession according to the information Alice sends to him, thereby attempting to recreate the initial target state. We quantify the quality of the protocol by the modulus square of the inner product between the target state and the actual state that Bob reconstructs. This quantity is known as the *fidelity*.

The fidelity has an important interpretation in quantum measurement theory which makes it a particularly appropriate measure of the quality of a teleportation protocol. Consider for a moment how Bob and Alice would establish that the protocol had succeeded. If two physical systems are in the same pure quantum state, then the statistics of all possible measurements made on those systems must be the same. In reality of course we cannot measure every physical quantity. The question of how many measurements suffice has been the subject of considerable research and forms the basis of quantum state tomography [41]. To assess how well the teleportation protocol has worked we essentially need to know the statistical distinguishability of the actual state $|\psi\rangle_a$ achieved and the ideal state $|\psi\rangle_i$. The answer to this question is known. The statistical distance between two classical distributions, $p_n^{(1)}, p_n^{(2)}$ is given in terms of the classical fidelity by

$$F(p^{(1)}, p^{(2)}) = \sum_n \sqrt{p_n^{(1)}, p_n^{(2)}} \quad (4)$$

If we now minimise this over all possible measurement distributions, we find it is bounded from below by the quantum fidelity [45].

The fidelity of quantum teleportation protocol is determined by the degree of shared entanglement, the quality of the measurements made by the sender, the quality of the classical communication channels used and finally it depends on how well Bob can implement the desired unitary transformations. In this paper we will discuss only

the first of these; the amount of shared entanglement. In the original teleportation protocol [8], the bipartite system was made up of two systems each described by a two dimensional Hilbert space, that is to say, two qubits, and the shared entangled state was a *maximally* entangled state [42]. In the case of two correlated harmonic oscillators, or two field modes, we cannot define maximal entanglement in quite the same way, as the entropy of each component system can be arbitrarily large. In this paper we define extremal entangled pure states of two field modes in terms of the total mean photon number and the total maximum photon number.

In the case of a system with a finite dimensional Hilbert space, a state of maximum entropy is simply the identity operator in that Hilbert space. A natural generalisation of this idea to infinite Hilbert spaces would define a maximum entropy state subject to some constraint, such as mean energy or total energy. These of course define the canonical ensemble and micro canonical ensemble of statistical mechanics. In the case of entangled pure states the Araki-Lieb [43] inequality indicates that the entropy of each component system is equal. As the entropy of a harmonic oscillator scales with mean energy, this indicates that each component subsystem has the same mean energy. If we maximise the entropy of each subsystem subject to a constraint on the mean energy, the state must be a thermal state. The entangled pure two mode state for which the reduced density operator of each mode is thermal is the squeezed vacuum state.

$$|\lambda\rangle = (1 - \lambda^2)^{-1/2} \sum_{n=0}^{\infty} \lambda^n |n, n\rangle \quad (5)$$

The mean photon number in each mode is given by $\bar{n} = \lambda^2/(1 - \lambda^2)$. If however we constrain the total photon number, N , of each mode we get a very different definition of an entangled our state,

$$|N\rangle = \frac{1}{\sqrt{1+N}} \sum_{n=0}^N |N - n, n\rangle \quad (6)$$

The entropy of the reduced state of each mode is $\ln(1+N)$ while the mean photon number is $N/2$. We will consider n of these entangled pre-states as a teleportation resource. While squeezed vacuum states may be achieved in the laboratory, states with fixed total photon number have not been produced, and will not be possible until we have a reliable N photon source. There are now a couple of proposals for such sources [44] and it may not be too long before they are used in teleportation schemes.

Teleportation fidelity for infinite dimensional Hilbert spaces must necessarily vary from unity for an arbitrary target state, as the notion of a maximally entangled resource differs from the finite dimensional case. The teleportation protocol can also be degraded by unknown incoherent process that corrupts the purity of the shared entanglement see Figure 2. Of course in some cases

these incoherent processes may destroy the correlations entirely, for example by absorbing all the photons in each mode before Alice and Bob get to use them. In this paper, however, we will only consider those decoherence processes that change the purity of the states and leave unchanged the classical intensity correlations.

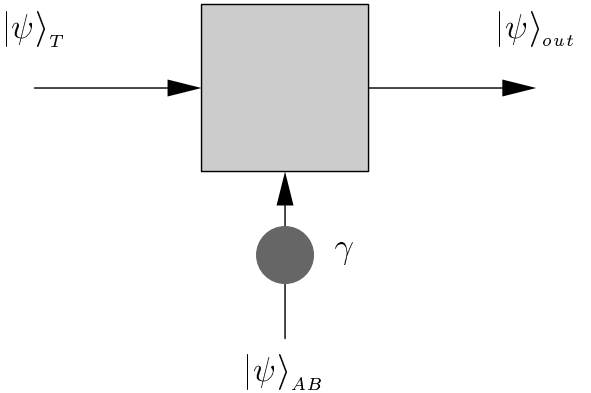


FIG. 2. Using teleportation to analyse entanglement. The decoherence process (grey circle) affects the entanglement resource $|\psi\rangle_{AB}$ thereby changing the overlap between $|\psi\rangle_T$ and $|\psi\rangle_{out}$ after the teleportation protocol (grey box).

III. IDEAL RESOURCE

In a recent paper by Milburn and Braunstein [33] a teleportation protocol was presented using joint measurements of the photon number difference and phase sum on two field modes. This protocol is possible because the number difference and phase sum operators commute, thus allowing determination of these quantities simultaneously and to arbitrary accuracy. The teleportation scheme improves with increasing number of Fock states in the resource since the resource states tend to simultaneous eigenstates of number difference and phase sum.

Number *sum* and phase *difference* operators also commute, implying that if eigenstates of these operators can be found a teleportation protocol is possible. Such a protocol is discussed below.

Because the number sum and phase difference operators commute we look for simultaneous eigenstates of these observables. Consider states of the form

$$|\psi\rangle_{AB} = \sum_{n=0}^N d_n |N - n\rangle_A |n\rangle_B \quad (7)$$

which are eigenstates of number sum with eigenvalue N . The labels A and B refer to Alice's and Bob's modes respectively and the coefficients d_n satisfy $\sum_{n=0}^N |d_n|^2 = 1$, so that the state is normalised. For Eq. (7) to be used as a resource for teleportation it needs to be entangled; it will be maximally entangled when the d_n are all equal. We choose $d_n = \frac{1}{\sqrt{N+1}}$, giving the resource,

$$|\psi\rangle_{AB} = \frac{1}{\sqrt{N+1}} \sum_{n=0}^N |N-n\rangle_A |n\rangle_B. \quad (8)$$

This resource tends towards eigenstates of phase difference as $N \rightarrow \infty$. To see this consider the joint phase probability density of Eq. (8), which is calculated by projecting onto each mode with the phase state, [47–49]

$$|\phi\rangle = \sum_{n=0}^{\infty} e^{in\phi} |n\rangle, \quad (9)$$

and taking the modulus squared, i.e.,

$$\begin{aligned} P(\phi_A, \phi_B) &= |\langle \phi_A | \langle \phi_B | \psi_{AB} \rangle|^2 \\ &= \frac{1}{\sqrt{N+1}} \left| \sum_{n=0}^N e^{in\phi_-} \right|^2 \end{aligned} \quad (10)$$

where $\phi_- = \phi_A - \phi_B$. The probability density as a function of N and ϕ_- is shown in Figure 3, and shows that as N gets larger this density becomes sharply peaked about $\phi_- = 0$ in the interval $[-\pi, \pi]$, hence the states of Eq. (8) tend to eigenstates of phase difference with increasing N .

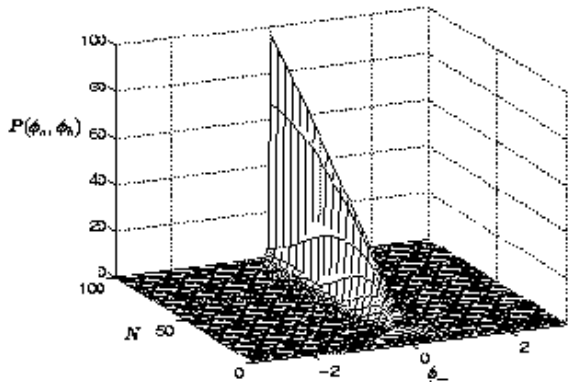


FIG. 3. Joint phase probability density. As N increases the probability density becomes very narrowly peaked about $\phi_- = 0$.

To decide when N is sufficiently large for the resource (Eq. (8)) to be called a simultaneous eigenstate of phase difference we need to determine when the probability density (Eq. (10)) is sufficiently narrow. We make the criterion that if the full width at half maximum of the density is 1% of the domain of ϕ_- ($[-\pi, \pi]$) then N is large enough. This criterion is met if $N > 88$.

The state to be teleported can be written in the general form

$$|\psi\rangle_T = \sum_{m=0}^{\infty} c_m |m\rangle_T, \quad (11)$$

The subscript T is used to emphasise that this is the “target” mode. We generate the input state to the protocol by taking the tensor product of the target and the resource

$$\begin{aligned} |\psi\rangle_{TAB} &= |\psi\rangle_T \otimes |\psi\rangle_{AB} \\ &= \frac{1}{\sqrt{N+1}} \sum_{m=0}^{\infty} \sum_{n=0}^N c_m |m\rangle_T |N-n\rangle_A |n\rangle_B. \end{aligned} \quad (12)$$

Alice’s measurement of the number sum on the target and her mode projects the input state into the conditional state

$$\begin{aligned} |\psi^{(q)}\rangle &= \frac{1}{\sqrt{N+1}} \frac{1}{\sqrt{P_I(q)}} \\ &\times \sum_n c_{q-N+n} |q-N+n\rangle_T |N-n\rangle_A |n\rangle_B, \end{aligned} \quad (13)$$

where n runs from $\max(0, N-q)$ to N , and q is the number sum measurement result, and

$$P_I(q) = \frac{1}{N+1} \sum_n |c_{q-N+n}|^2, \quad (14)$$

is the probability of measuring that result, I merely emphasises that this probability relates to the idealised resource Eq. (8). Note that again the summation runs from $n = \max(0, N-q)$ to N . After Alice’s measurement of the phase difference the total state is

$$\begin{aligned} |\psi^{(q, \phi_-)}\rangle &= e^{i(q-2N)\phi_-} \\ &\times \sum_{w,y=0}^{\infty} e^{i(y-w)\phi_-} \delta_{w,q-y} |w\rangle_T |y\rangle_A \\ &\otimes \frac{1}{\sqrt{N+1}} \frac{1}{\sqrt{P_I(q)}} \\ &\times \sum_n e^{2in\phi_-} c_{q-N+n} |n\rangle_B, \end{aligned} \quad (15)$$

implying that the state in Bob’s mode is

$$\begin{aligned} |\psi\rangle_B &= \frac{1}{\sqrt{N+1}} \frac{1}{\sqrt{P_I(q)}} \\ &\times \sum_n e^{2in\phi_-} c_{q-N+n} |n\rangle_B. \end{aligned} \quad (16)$$

Using the results q and ϕ_- , and knowledge of the number of Fock states in the resource (N), Bob has sufficient information to reproduce the target state. He does this by amplifying his mode so that $|n\rangle_B \rightarrow |q-N+n\rangle_B$ and phase shifting it by $e^{-i2n\phi_-}$. The unitary amplification operation is described in [50]. These operations complete the protocol and the state Bob finally has in his possession is

$$\begin{aligned} |\psi\rangle_{out, B} &= \frac{1}{\sqrt{N+1}} \frac{1}{\sqrt{P_I(q)}} \\ &\times \sum_n c_{q-N+n} |q-N+n\rangle_B. \end{aligned} \quad (17)$$

The fidelity of this protocol is

$$F_I = \sum_n |c_{q-N+n}|^2. \quad (18)$$

To see how well the teleportation protocol performs, let us consider some examples.

1. Example: Target is a number state

Let the target state be a number state,

$$|\psi\rangle_T = |m\rangle_T, \quad (19)$$

so the only coefficient available is c_m , which is one.

We find that the teleportation fidelity is unity, independent of the measurement of q , because the only term appearing in the summations of both the fidelity and the probability is that corresponding to c_m . Therefore, this protocol works perfectly if the target is a number state.

2. Example: Target is a coherent state

The fidelity as a function of number sum measurement, q , and number of Fock states in the resource minus one, N , for a coherent target state of amplitude, $\alpha = 3$, is displayed in Figure 4.

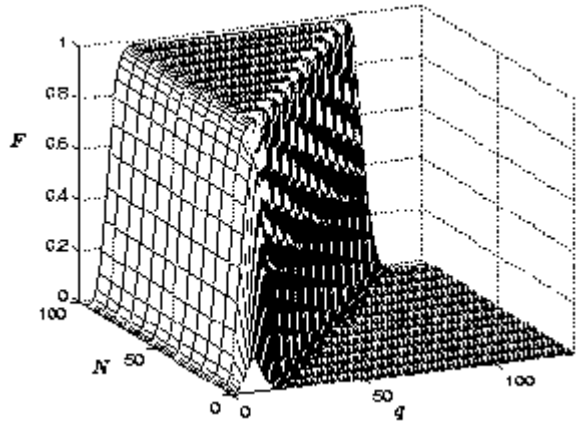


FIG. 4. Fidelity, F , as a function of number sum measurement, q , and energy in the ideal resource, N , for a coherent state of amplitude $\alpha = 3$.

The figure shows that as N increases, the range of measurement outcomes of number sum measurements for which the fidelity is high also increases, implying the technique is improving with increasing N . Also consider the probability of finding a given q , which is shown as a function of q and N in Figure 5. This shows that the probability of obtaining a given number sum is high in correspondence with the ranges of q for which the fidelity is high. Hence we can say that the protocol works well as result of this correspondence.

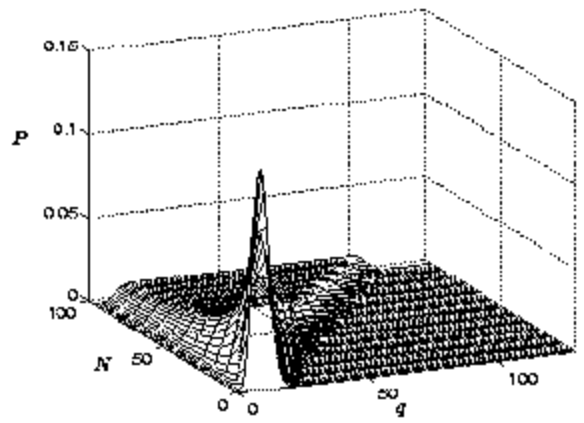


FIG. 5. Probability, P , as a function of number sum measurement, q , and energy in the ideal resource, N , for a coherent state of amplitude $\alpha = 3$.

We expect this protocol to improve with increasing N for two reasons: the approach of the resource states to simultaneous eigenstates of number sum and phase difference, and an improved resolution of the target state. Firstly, as mentioned in Section III, as N increases the resource states tend to eigenstates of phase difference and since they are already eigenstates of number sum they therefore tend to simultaneous eigenstates of both quantities. Because of this the joint measurements of number sum and phase difference made by Alice become more accurate which we would expect to improve the output of the teleportation. Secondly, the resolution of the target improves with increasing N . What we mean is that there are more states available in the resource with which to “encode” the target before it is teleported. An analogy between this and digital electronics can be made. Consider an analogue to digital converter. Such a device converts (“encodes”) a continuous analogue signal into a digital form in much the same way we do in our teleportation protocol. The quality of the digital reproduction of the analogue signal increases as one increases the number of bits one uses to “encode” the analogue signal in the digital medium. Much the same process occurs here where as we add more states to the description of our resource (i.e. increase N) we are increasing the number of “bits” used to “encode” the target state. We use the words “bit” and “encode” very loosely, but the idea is what is important. So, in analogy with the analogue to digital converter, as we increase the number of “bits” in our resource we would also expect the quality of output (fidelity) to improve. Overall, this implies that the shape of the fidelity function in Figure 4 is not surprising, and in fact what we would expect.

IV. BEAM SPLITTER RESOURCE

The resource states discussed in Section III illustrate the protocol well, but do not describe a known physical

interaction. However the beam splitter interaction can be shown to give a resource with similar properties to Eq. (8). The beam splitter interaction is described by [51]

$$|\psi\rangle_{AB} = e^{i\frac{\pi}{4}(a^\dagger b + ab^\dagger)}|N\rangle_A|N\rangle_B, \quad (20)$$

where the operators a , a^\dagger , b and b^\dagger are the usual boson annihilation and creation operators for modes A and B . N is the number of photons at each port of the beam splitter.

We can understand these states by considering the boson representation of SU(2) algebra;

$$\hat{J}_x = \frac{1}{2}(a^\dagger b + b^\dagger a) \quad (21a)$$

$$\hat{J}_y = \frac{-i}{2}(a^\dagger b - b^\dagger a) \quad (21b)$$

$$\hat{J}_z = \frac{1}{2}(a^\dagger a - b^\dagger b) \quad (21c)$$

$$\hat{J}^2 = N(N+1). \quad (21d)$$

Let us restrict the state space to eigenstates of the number sum such that $a^\dagger a + b^\dagger b = 2N$, implying a pseudo angular momentum algebra. The eigenstates of \hat{J}_z can be written in the number state basis as

$$|N, \mu\rangle_z = |N + \mu\rangle_A|N - \mu\rangle_B. \quad (22)$$

There are $2N + 1$ such eigenstates with eigenvalues $\mu = -2N, -2N + 1, \dots, 0, \dots, 2N - 1, 2N$. Consequently, we can write Eq. (20) in the form

$$|\psi\rangle_{AB} = e^{i\frac{\pi}{2}\hat{J}_x}|N, 0\rangle_z. \quad (23)$$

Expanding this in terms of the \hat{J}_z eigenstates in the Fock basis we obtain,

$$|\psi\rangle_{AB} = \sum_{\mu=-N}^N {}_z\langle N, \mu|e^{i\frac{\pi}{2}\hat{J}_x}|N, 0\rangle_z \times |N + \mu\rangle_A|N - \mu\rangle_B, \quad (24)$$

where the term ${}_z\langle N, \mu|e^{i\frac{\pi}{2}\hat{J}_x}|N, 0\rangle_z$ is the distribution of the \hat{J}_z eigenstates over the range $-N \leq \mu \leq N$ and can be obtained from the rotation matrix coefficients (which are discussed in more detail in Appendix (B)). Eq. (24) is written more simply as

$$|\psi\rangle_{AB} = \sum_{n=0}^{2N} d_{n-N}|n\rangle_A|2N - n\rangle_B. \quad (25)$$

where the d_{n-N} are the rotation matrix coefficients and making the change of variables $\mu = n - N$. These states may be used as a resource in our number sum, phase difference teleportation protocol because their form is very similar to Eq. (7). This protocol proceeds identically to that discussed in Section III excepting the additional

knowledge of how the the resource is generated and the inherent properties therein.

We illustrate this variation of the protocol with the pure state form of the resource as given in Eq. (25). The total state is,

$$|\psi\rangle_{TAB} = |\psi\rangle_T \otimes |\psi\rangle_{AB} = \sum_{m=0}^{\infty} \sum_{n=0}^{2N} c_m d_{n-N} |m\rangle_T |n\rangle_A |2N - n\rangle_B. \quad (26)$$

The state of the system, conditioned on the number sum result q , is

$$|\psi^{(q)}\rangle = \mathcal{N}_{BS} \sum_{n=0}^{\min(q, 2N)} c_{q-n} d_{n-N} \times |q - n\rangle_T |n\rangle_A |2N - n\rangle_B, \quad (27)$$

where $\mathcal{N}_{BS} = \frac{1}{\sqrt{P_{BS}(q)}}$ and

$$P_{BS}(q) = \sum_{n=0}^{\min(q, 2N)} |c_{q-n}|^2 |d_{n-N}|^2, \quad (28)$$

is the probability of obtaining the result q , the subscript denoting that the probability is for the beam splitter generated resource. After phase difference measurement the total state is,

$$|\psi^{(q, \phi_-)}\rangle = \sum_{w, y=0}^{\infty} e^{i(y - w - q)\phi_-} \delta_{w, q-y} |w\rangle_T |y\rangle_A \otimes \mathcal{N}_{BS} \sum_{n=0}^{\min(q, 2N)} e^{2in\phi_-} \times c_{q-n} d_{n-N} |2N - n\rangle_B, \quad (29)$$

and the state in Bob's mode is

$$|\psi\rangle_B = \mathcal{N}_{BS} \sum_{n=0}^{\min(q, 2N)} e^{2in\phi_-} \times c_{q-n} d_{n-N} |2N - n\rangle_B. \quad (30)$$

Applying the amplification $|2N - n\rangle_B \rightarrow |q - n\rangle_B$ and the phase shift $e^{-2in\phi_-}$, the output state becomes,

$$|\psi\rangle_{out, B} = \mathcal{N}_{BS} \sum_{n=0}^{\min(q, 2N)} c_{q-n} d_{n-N} |q - n\rangle_B, \quad (31)$$

and the teleportation fidelity is found to be

$$F_{BS} = \frac{1}{P_{BS}(q)} \left| \sum_{n=0}^{\min(q, 2N)} |c_{q-n}|^2 d_{n-N} \right|^2. \quad (32)$$

3. Example: Target is a coherent state

The fidelity function in Figure 6 is almost identical to Figure 4 except that its maximum is one half as opposed to unity. The reason for this is due to every second term of the target is being removed because the every second term of the resource is zero. Every second term of the resource is zero because in the case of equal photon number incident onto each port of a 50:50 beam splitter gives rotation matrix coefficients whose every second term is zero. Therefore, only half of the terms in the target are contributing to the fidelity, so the maximum the fidelity can be for such a target is one half. As in the ideal case, this resource improves in its ability to teleport a state with increasing N for exactly the same reasons discussed in Section III

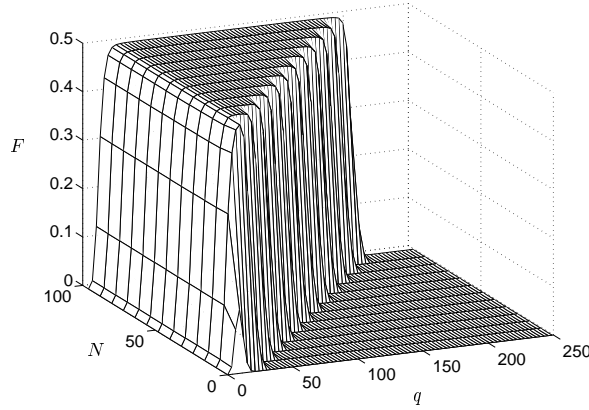


FIG. 6. Fidelity, F , as a function of number sum measurement, q , and energy in the beamsplitter resource, N , for a coherent state of amplitude $\alpha = 3$.

The probability function is shown in Figure 7 and has much the same structure as the probability in Figure 5. The “bumps” on the “edge” of the surface are due to the distribution of the d_{n-N} coefficients not being flat (c.f. the even distribution of Eq. (8)).

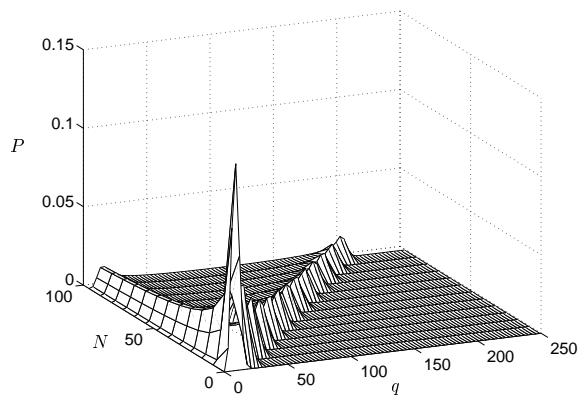


FIG. 7. Probability, P , as a function of number sum measurement, q , and energy in the beamsplitter resource, N , for a coherent state of amplitude $\alpha = 3$.

4. Example: Target is an even “cat” state

If we have some *a priori* knowledge about the form of the state we are attempting to teleport, it is possible to achieve unit fidelity. For instance if we use an even “cat” state, formed from the superposition of two coherent states of equal amplitude but opposite sign, [52]

$$|\psi\rangle_T = \frac{|\alpha\rangle_T + |-\alpha\rangle_T}{\sqrt{2 + 2e^{-2|\alpha|^2}}}, \quad (33)$$

we find that every second term of the target is zero. This means that even though every second term in the resource is zero and is removing every second term from the target, this has no effect on the resource’s ability to teleport an even “cat” state, as shown by the fidelity function in Figure 8.

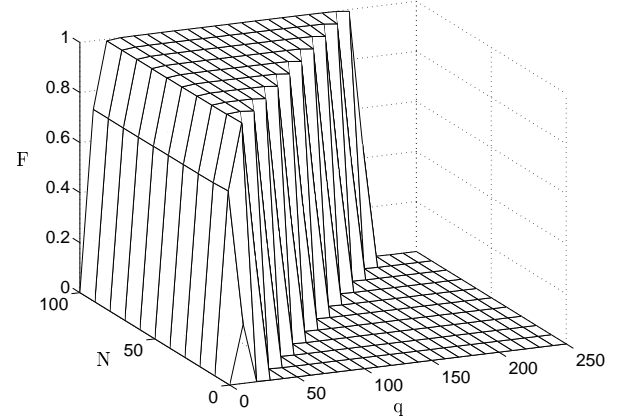


FIG. 8. Fidelity, F , as a function of number sum measurement, q , and energy in the beamsplitter resource, N , for a “cat” state of amplitude $\alpha = 3$.

This example is interesting since we have seemingly added only a small amount of extra information but we have greatly improved the quality of the protocol. Even such incomplete knowledge about the target as its parity or form in a given basis can allow one to teleport the state perfectly with a seemingly imperfect resource. This result implies that it is possible to tailor resources for given applications, so that if only the form of the state to be teleported is known, then one may be able to construct a resource that will teleport the state perfectly, without the resource necessarily being able to teleport an arbitrary state perfectly.

V. DECOHERENCE

We model decoherence by using phase diffusion. This retains the classical (number or intensity) correlations in the system, but alters the quantum (entanglement related) correlations. Phase diffusion is modelled by applying the following phase shift to the resource

$$U(\theta) \equiv \exp [-i(\theta_a a^\dagger a + \theta_b b^\dagger b)], \quad (34)$$

where the combined phase of θ_a and θ_b is taken to be Gaussian randomly distributed with a zero mean and variance σ .

$$P(\theta) = \frac{1}{\sqrt{2\pi\sigma}} \exp \left(-\frac{\theta^2}{2\sigma} \right). \quad (35)$$

Even though a Gaussian distribution is not periodic it can be taken to be an approximation to a true periodic distribution, such as $\cos^{2N}(\theta - \theta_0)$, for sufficiently large N . To see that this is so, consider the probability distribution

$$P(\theta) = \mathcal{N} \cos^{2N}(\theta - \theta_0) \quad (36)$$

where \mathcal{N} is the normalisation. This can be approximated by

$$\begin{aligned} P(\theta) &\approx \mathcal{N} \left[1 - \frac{(\theta - \theta_0)^2}{2} \right]^{2N} \\ &\approx \mathcal{N} [1 - N(\theta - \theta_0)^2] \\ &\approx \mathcal{N} \exp [-N(\theta - \theta_0)^2] \\ &= \mathcal{N} \exp \left[-\frac{1}{2} \frac{(\theta - \theta_0)^2}{\sigma} \right] \end{aligned} \quad (37)$$

where $\sigma = \frac{1}{2N}$. Therefore, a Gaussian distribution can approximate a true periodic distribution given the condition that $\sigma \sim \frac{1}{2N}$.

A. Squeezed state resource

The phase diffusion model may be illustrated by applying it to the resource discussed by Milburn and Braunstein [33]. In their paper they describe teleportation using two-mode squeezed vacuum states as an entanglement resource for teleportation. The entanglement between resource modes may be altered by changing the squeezing parameter, λ , and by decohering the resource using phase diffusion. The resource for this protocol is written in the Fock basis as

$$|\psi\rangle_{AB} = \sqrt{1 - \lambda^2} \sum_{n=0}^{\infty} \lambda^n |n\rangle_A |n\rangle_B. \quad (38)$$

Applying the phase shift $U(\theta)$ to the resource gives,

$$\begin{aligned} |\psi(\theta)\rangle_{AB} &= \sqrt{1 - \lambda^2} e^{-i(\theta_a a^\dagger a + \theta_b b^\dagger b)} \sum_{n=0}^{\infty} \lambda^n |n\rangle_A |n\rangle_B \\ &= \sqrt{1 - \lambda^2} \sum_{n=0}^{\infty} e^{-i\theta n} \lambda^n |n\rangle_A |n\rangle_B, \end{aligned} \quad (39)$$

where $\theta = \theta_a + \theta_b$ is the Gaussian distributed random variable with mean zero and variance σ

We average over all realisations of the phase to give the resource as a density operator

$$\begin{aligned} \rho_{AB} &= (1 - \lambda^2) \sum_{n,n'=0}^{\infty} \lambda^n \lambda^{n'} e^{-\gamma(n-n')^2} \\ &\quad \times |n\rangle_A \langle n'| \otimes |n\rangle_B \langle n'|, \end{aligned} \quad (40)$$

where γ describes the degree of decoherence and is equal to $\sigma/2$. The input state is

$$\begin{aligned} \rho_{TAB} &= \rho_T \otimes \rho_{AB} \\ &= (1 - \lambda^2) \sum_{n,n'=0}^{\infty} c_m c_{m'}^* \lambda^n \lambda^{n'} e^{-\gamma(n-n')^2} \\ &\quad \times |m\rangle_T \langle m'| \otimes |n\rangle_A \langle n'| \otimes |n\rangle_B \langle n'|. \end{aligned} \quad (41)$$

This teleportation takes two paths, one characterised by measurement of a positive number difference and one by a negative number difference. We will arrive at two fidelities, each corresponding to the relevant measurement.

1. Positive number difference measurement

The state conditioned on the positive number difference, q is

$$\begin{aligned} \rho_{+}^{(q)} &= \frac{1 - \lambda^2}{P_{+}(q)} \sum_{n,n'=0}^{\infty} c_{n+q} c_{n'+q}^* \lambda^n \lambda^{n'} e^{-\gamma(n-n')^2} \\ &\quad \times |n+q\rangle_T \langle n+q| \otimes |n\rangle_A \langle n'| \otimes |n\rangle_B \langle n'|, \end{aligned} \quad (42)$$

where

$$P_{+}(q) = (1 - \lambda^2) \sum_{n=0}^{\infty} |c_{n+q}|^2 \lambda^{2n}, \quad (43)$$

is the probability of finding the result q . After measurement of the phase sum the system is in the state

$$\begin{aligned} \rho^{(q,\phi_+)} &= \sum_{x,y,x',z'=0}^{\infty} e^{i(w+y-x'-z')\phi_+} \delta_{w,q+y} \delta_{q,x'-z'} \\ &\quad \times |w\rangle_T \langle x'| \otimes |y\rangle_A \langle z'| \\ &\otimes \frac{1 - \lambda^2}{P_{+}(q)} \sum_{n,n'=0}^{\infty} e^{-2i(n-n')\phi_+} c_{n+q} c_{n'+q}^* \\ &\quad \times \lambda^n \lambda^{n'} e^{-\gamma(n-n')^2} |n\rangle_B \langle n'|, \end{aligned} \quad (44)$$

so the state in Bob's mode is

$$\rho_B = \frac{1 - \lambda^2}{P_+(q)} \sum_{n,n'=0}^{\infty} e^{-2i(n-n')\phi_+} c_{n+q} c_{n'+q}^* \\ \times \lambda^n \lambda^{n'} e^{-\gamma(n-n')^2} |n\rangle_B \langle n'|. \quad (45)$$

After amplification and phase shifting the output state is

$$\rho_{out,B} = \frac{1 - \lambda^2}{P_+(q)} \sum_{n,n'=0}^{\infty} c_{n+q} c_{n'+q}^* \\ \times \lambda^n \lambda^{n'} e^{-\gamma(n-n')^2} |n+q\rangle_B \langle n'+q|, \quad (46)$$

with a corresponding fidelity given by

$$F_+ = \frac{1 - \lambda^2}{P_+(q)} \sum_{n,n'=0}^{\infty} |c_{n+q}|^2 |c_{n'+q}|^2 \lambda^n \lambda^{n'} e^{-\gamma(n-n')^2}, \quad (47)$$

2. Negative number difference measurement

For measurement of negative number difference, $q' = -q$, the conditional state is

$$\rho_{-}^{(q')} = \frac{1 - \lambda^2}{P_{-}(q')} \sum_{m,m'=0}^{\infty} c_m c_{m'}^* \lambda^{m+q'} \lambda^{m'+q'} e^{-\gamma(m-m')^2} \\ \times |m\rangle_T \langle m'| \otimes |m+q'\rangle_A \langle m'+q'| \\ \otimes |m+q'\rangle_B \langle m'+q'|, \quad (48)$$

where

$$P_{-}(q') = (1 - \lambda^2) \sum_{m=0}^{\infty} |c_m|^2 \lambda^{2(m+q')}, \quad (49)$$

is the probability of obtaining the result q' . The fidelity after teleportation is

$$F_{-} = \frac{1 - \lambda^2}{P_{-}(q')} \sum_{m,m'=0}^{\infty} |c_m|^2 |c_{m'}|^2 \lambda^{m+q'} \lambda^{m'+q'} e^{-\gamma(m-m')^2}. \\ (50)$$

The fidelity as a function of q and γ is shown in Figure 9 and behaves as we would expect, decoherence in the resource reduces the output quality of the protocol implying that the entanglement available as a resource for teleportation has decreased.

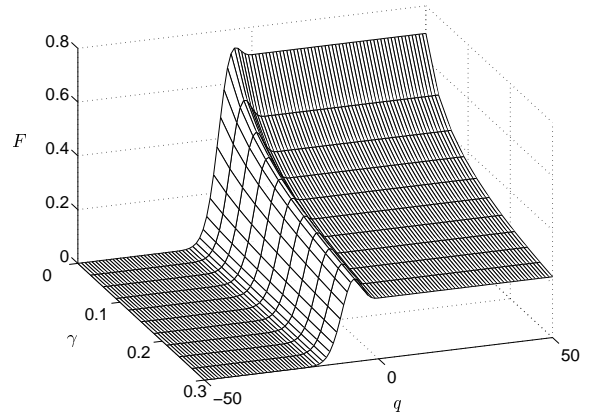


FIG. 9. Fidelity as a function of number difference measurement, q , and degree of decoherence, γ , with a squeezing parameter value of $\lambda = 0.8$ at a two-mode squeezed state resource energy corresponding to $N = 100$.

If we take $\gamma = 0$ and a coherent state of amplitude $\alpha = 6$ then we can reproduce the results of Ref. [33].

B. Ideal resource

Applying our decoherence model to Eq. (8) and averaging over all realisations of the phase we obtain the total state:

$$\rho_{TAB} = \frac{1}{N+1} \sum_{m,m'=0}^{\infty} \sum_{n,n'=0}^N c_m c_{m'}^* e^{-\gamma(n-n')^2} \\ \times |m\rangle_T \langle m'| \otimes |N-n\rangle_A \langle N-n'| \otimes |n\rangle_B \langle n'| \quad (51)$$

where γ is the degree of decoherence as before. After completion of the protocol the fidelity is given by

$$F_{I,\gamma} = \frac{1}{N+1} \frac{1}{P_I(q)} \sum_{n,n'} |c_{q-N+n}|^2 |c_{q-N+n'}|^2 e^{-\gamma(n-n')^2}. \\ (52)$$

where n and n' run from $\max(0, N - q)$ to N and

$$P_I(q) = \frac{1}{N+1} \sum_n |c_{q-N+n}|^2, \quad (53)$$

is the probability of obtaining the result q as obtained in Eq. (14). It is not difficult to show that by letting $\gamma = 0$ we reproduce the result without noise, Eq. (18).

Let us examine the example of a coherent state, $\alpha = 3$. The fidelity as a function of γ and q is shown in Figure 10 and shows how decoherence affects the fidelity. As the degree of decoherence (γ) is increased, the fidelity drops away very quickly. This is because the off-diagonal matrix elements of ρ_{AB} are being “washed out” by the $(n - n')^2$ term in the exponential. Physically, we are reducing the entanglement between the resource modes by

making measurement of phase more random and would expect the ability of the technique to teleport a state to decrease – Figure 10 shows this effect explicitly.

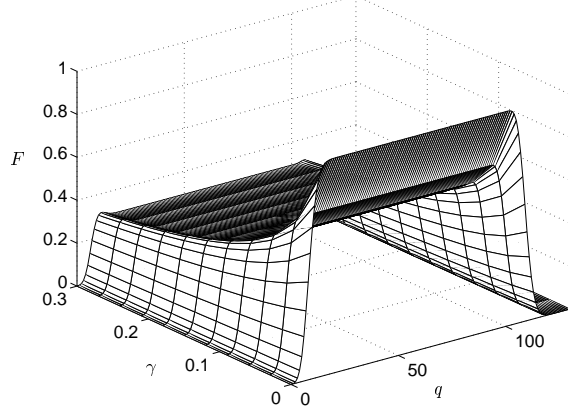


FIG. 10. Fidelity as a function of number sum measurement, q , and degree of decoherence, γ , with an ideal resource energy corresponding to $N = 100$.

C. Beam splitter resource

We add noise to the beam splitter resource state in the same manner as described in Section V A, obtaining the total state,

$$\rho_{TAB} = \sum_{m,m'=0}^{\infty} \sum_{n,n'=0}^{2N} c_m c_{m'}^* d_{n-N} d_{n'-N}^* e^{-\gamma(n-n')^2} \times |m\rangle_T \langle m'| \otimes |n\rangle_A \langle n'| \otimes |2N-n\rangle_B \langle 2N-n'|. \quad (54)$$

After the teleportation protocol, we find that the fidelity with respect to the initial state is given by

$$F_{BS,\gamma} = \frac{1}{P_{BS}(q)} \sum_{n,n'=0}^{\min(q,2N)} |c_{q-n}|^2 |c_{q-n'}|^2 \times d_{n-N} d_{n'-N}^* e^{-\gamma(n-n')^2}. \quad (55)$$

where

$$P_{BS}(q) = \sum_{n=0}^{\min(q,2N)} |c_{q-n}|^2 |d_{n-N}|^2, \quad (56)$$

is the probability of obtaining the number sum result q .

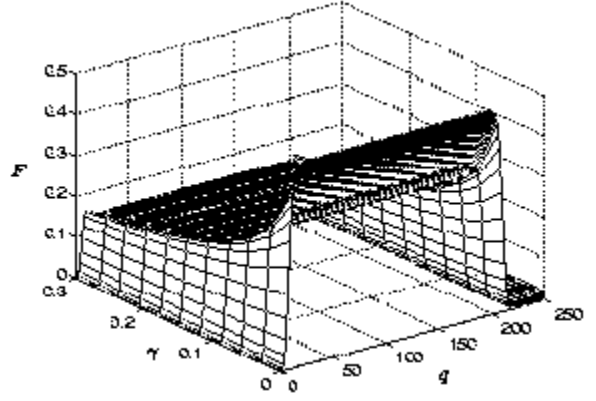


FIG. 11. Fidelity as a function of number sum measurement, q , and degree of decoherence, γ , with a beamsplitter resource energy corresponding to $N = 100$.

Again, the fidelity decreases due to decoherence in the resource, except that the fidelity decreases from one half instead of one as in Section III.

VI. FULL DECOHERENCE

Full decoherence corresponds to no entanglement between the resource modes and a completely flat phase probability distribution. A flat phase probability distribution is equivalent to taking the limit $\gamma \rightarrow \infty$ in the fidelities of Section V making the off-diagonal terms in the density matrix representing the output state $\rho_{out,B}$ zero. Physically, this limit corresponds to retaining the number correlations but making a measurement of phase completely arbitrary. We take this limit for each of the three cases discussed in Section V.

A. Idealised resource

A fully decohered resource implies Eq. (52) reduces to

$$F_{I,\infty} = \frac{1}{N+1} \frac{1}{P_I(q)} \sum_{n=\max(0,N-q)}^N |c_{q-N+n}|^4. \quad (57)$$

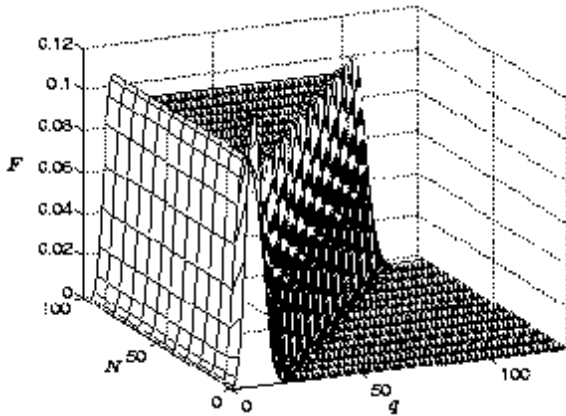


FIG. 12. Fidelity as a function of number sum measurement, q , and energy in the fully decohered ideal resource, N , for a coherent state target of amplitude $\alpha = 3$.

$F_{I,\infty}$ as a function of q and N is shown in Figure 12, note that it behaves in much the same way as the noiseless case (Figure 4) where the fidelity stays “high” for an increasing part of the region of q with increasing N , but has a significantly lower value.

A feature of interest in Figure 12 is the bump on each edge of the fidelity distribution. As one scans across q for a given value of N the fidelity increases, drops from zero, peaks slightly to remain flat, then peaks again before dropping away to zero. These features may be seen more clearly in Figure 13 where $F_{I,\infty}$ is plotted against q for $N = 100$.

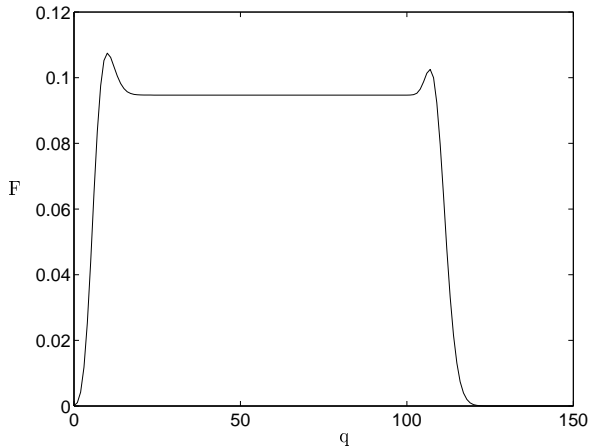


FIG. 13. Slice through fully decohered ideal resource fidelity function at $N = 100$.

The “bumps” are due to the distribution of the c_m coefficients of the input target state. To understand the origin of the “bumps” we write the fidelity of Eq. (57) more explicitly,

$$F_{I,\infty} = \frac{\sum_{n=\max(0, N-q)}^N |c_{q-N+n}|^4}{\sum_{n=\max(0, N-q)}^N |c_{q-N+n}|^2}. \quad (58)$$

Eq. (58) shows that we are finding the summation of a distribution with each term raised to the power of four divided by the same distribution with each term raised to the power of two. Note that a coherent state distribution squared has a larger spread than one raised to the power of four. The distributions for a coherent state, $\alpha = 3$ are shown in Figure 14. The α^2 curve corresponds to the coefficients of the coherent state squared and the α^4 curve corresponds to the coefficients raised to the power of four.

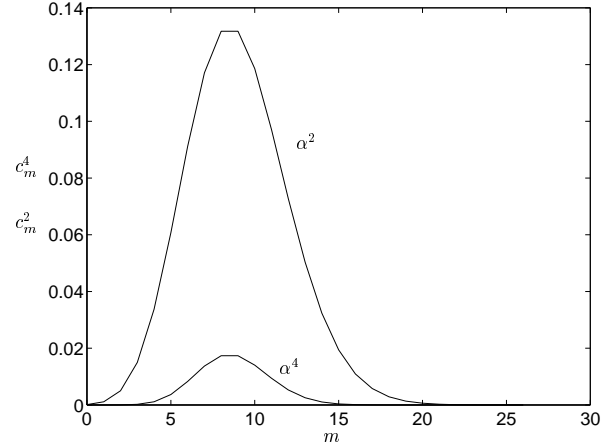


FIG. 14. Comparison of α^2 and α^4 coefficient distributions. The c_m are the values of the coefficients at a given value of the Fock number, m .

Let us consider $q < N$ in the range $m = [0, 2]$ which corresponds to the coefficients between c_0 and c_2 inclusive. The summations in Eq. (58) only add up the coefficients from c_0 to c_2 so, the major contribution to the fidelity comes from the α^2 curve which corresponds to the denominator in Eq. (58), hence the fidelity is small. If we let $m = 7$ the summations add about half of each of the two distributions, this corresponds to where the fidelity reaches about half of its maximum value in Figure 13. As we increase m further we are adding more of the α^4 distribution and the fidelity increases since this corresponds to the numerator in Eq. (58). Now take $m = 12$ which is where the α^4 distribution is small again, this corresponds to the maximum of the first “bump” in Figure 13. As we take larger m , the summation from c_0 to c_m of the α^4 distribution has maximised, but the summation of the α^2 distribution has not, so as we take larger m the fidelity decreases, since the α^2 distribution corresponds to the denominator in Eq. (58). The fidelity then stays at a constant value because both of the summations have reached their respective maxima. This tells us how the first “bump” is produced. The second “bump” is produced by exactly the same effect but in reverse order. At the m corresponding to the second “bump” we are in the region where $q > N$, hence the summation has changed from starting at c_0 and finishing at c_m , to starting at c_{q-N} and finishing at c_q . The summations now move as

a “window” of length $N + 1$ over the distributions. As the “window” moves across the distributions the contribution from the α^2 distribution decreases as coefficients are being dropped from the summation in the denominator, and we see the fidelity increase again, forming the second “bump”. As the “window” moves further to the right over the distributions in Figure 14 the fidelity drops away to zero as we are no longer adding non-zero terms in the two distributions.

One may notice that the “bump” on the right hand side of Figure 13 is lower than that on the left hand side. This is due to the distribution of states in the target. In the case that generates Figure 13 we are using a coherent state of amplitude three. The distribution of a coherent state of this amplitude is slightly asymmetrical and gives the slightly lower “bump” to the right we see in Figure 13. If we use a symmetric distribution of coefficients in the target state, say a Gaussian of the form,

$$c_n = \frac{1}{\sqrt{2\pi\sigma}} e^{-\frac{(n-n_0)^2}{2\sigma^2}}, \quad (59)$$

then one would expect to see the “bumps” occurring at the same height. This is exactly what we see in Figure 15, where we have used a Gaussian with n_0 arbitrarily set to 30 and $\sigma = 3$.

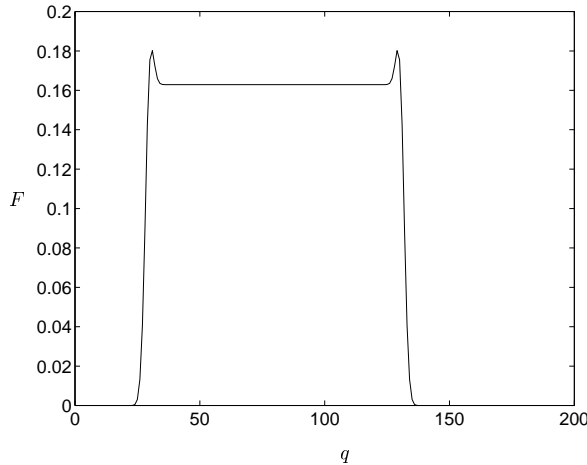


FIG. 15. Slice through fully decohered ideal resource fidelity function for a Gaussian distributed target at $N = 100$.

Because the “bumps” are due to differences in distribution width between when we square the terms in the distribution and when we take the terms in the distribution to the power of four, we would expect that if we choose a flat distribution then we would not see this effect. Take a target state with coefficients (in the Fock basis) defined by

$$\text{if } n < 57; \quad c_n = \frac{1}{4} \quad (60a)$$

$$\text{if } n \geq 40; \quad c_n = 0 \quad (60b)$$

The distribution of these coefficients squared will have the same width as that raised to the power of four. $F_{I,\infty}$

as a function of q and N for this distribution of coefficients is shown in Figure 16, note that it has no “bumps” as we expect. Hence we conclude that the “bumps” are a direct result of the continuous nature of the distribution of coefficients defining the target state.

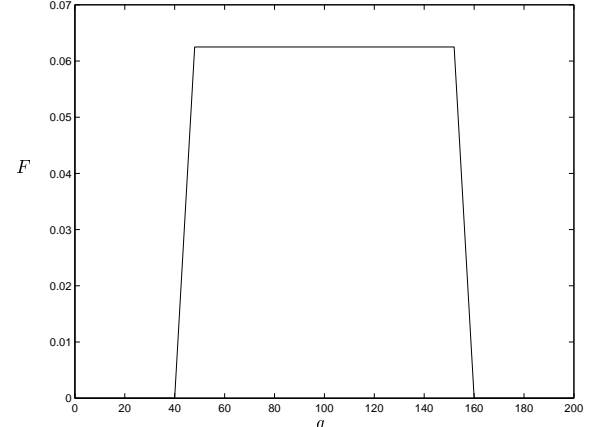


FIG. 16. Fidelity function of a fully decohered ideal resource for a flat target coefficient distribution.

B. Beam splitter resource

The fidelity for a fully decohered resource generated by the beam splitter interaction reduces from Eq. (55) to

$$F_{BS,\infty} = \frac{\sum_{n=0}^{\min(q,2N)} |c_{q-n}|^4 |d_{n-N}|^2}{\sum_{n=0}^{\min(q,2N)} |c_{q-n}|^2 |d_{n-N}|^2}. \quad (61)$$

This fidelity as a function of q and N is shown in Figure 17.

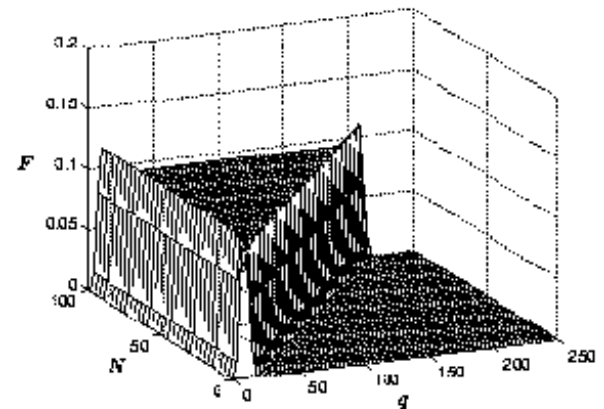


FIG. 17. Fidelity, F , as a function of number sum measurement, q , and energy in the fully decohered beam splitter resource, N , for a coherent state target of amplitude $\alpha = 3$.

Again, the typical trend of increasing region of high fidelity in q as N increases is shown. Notice that the constant value of the fidelity function when N is large is approximately that of the ideal case in Figure 12. One may wonder why this is so when previously the beam splitter version of the protocol could only achieve approximately half that of the ideal version. The reason for this is simple and can be explained by considering Eq. (61). In this equation both the numerator and denominator are setting half of the terms to zero (due to the zero terms of the rotation matrix coefficients) making the ratio almost identical to that in Eq. (57). Hence the maximum fidelities in the fully decohered limit are approximately the same for the ideal and beam splitter generated resources.

C. Squeezed state resource

The fidelities in the completely decohered limit reduce to

$$F_{+, \infty} = \frac{1 - \lambda^2}{P_+(q)} \sum_{n=0}^{\infty} |c_{n+q}|^4 \lambda^{2n} \quad (62)$$

and

$$F_{-, \infty} = \frac{1 - \lambda^2}{P_-(q')} \sum_{n=0}^{\infty} |c_n|^4 \lambda^{2(n+q')}. \quad (63)$$

and give us the surface in Figure 18

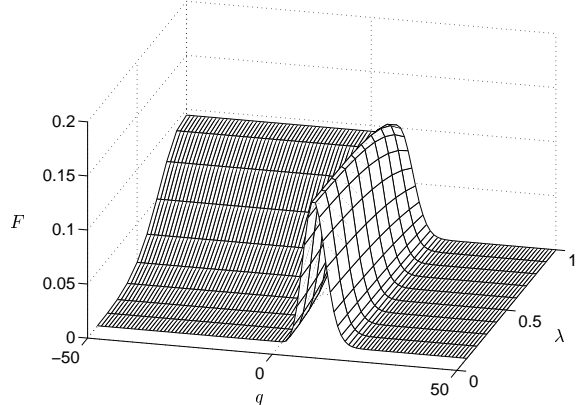


FIG. 18. Fidelity, F , as a function of number difference measurement, q , and squeezing parameter, λ for a fully decohered squeezed state resource. The target is a coherent state of amplitude $\alpha = 3$.

The surface we see in Figure 18 has the same form – except for being diminished in fidelity – as the squeezed state fidelity function over λ and q for no damping (Figure 19). Unfortunately, we have yet to come up with an adequate explanation as to why the top of the peak decreases as λ increases. Nevertheless, it is not difficult

to show that the position of the peak in q is determined by the target state. Here we use a coherent state of amplitude, $\alpha = 3$, which implies a peak value at $q = 9$, corresponding identically to Figure 18.

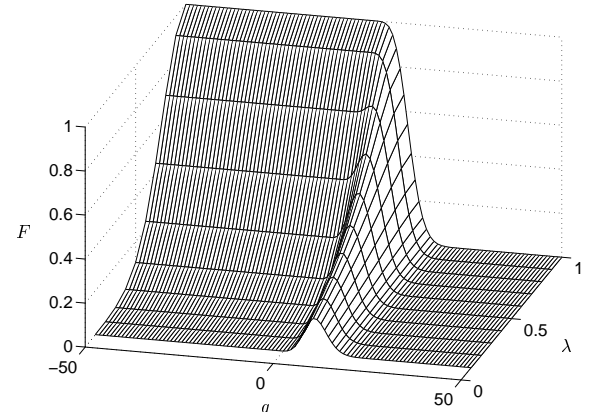


FIG. 19. Fidelity, F , as a function of number difference measurement, q , and squeezing parameter, λ , for a squeezed state resource without decoherence. The target is a coherent state of amplitude $\alpha = 3$.

VII. CONCLUSIONS

We have shown that a teleportation scheme involving coupled oscillator states using number sum and phase difference measurements is possible, given sufficiently large numbers of Fock states in the resource. The ability of the scheme to reliably teleport a state was shown to improve as the number of Fock state in the resource increases. In the case of the beam splitter generated resource this physically means more photons incident on the beam splitter ports. We have illustrated the effects of decoherence (in the form of phase diffusion) in three entanglement resources (ideal, beam splitter generated and squeezed state) on the fidelity of teleportation and have related this qualitatively to the change in entanglement of the resource. We have also shown that the ability of the resources to teleport a state increases with increase in the Fock space dimension.

ACKNOWLEDGMENTS

PTC acknowledges the financial support of the Centre for Laser Science and the University of Queensland Postgraduate Research Scholarship.

[2] L. K. Grover, Phys. Rev. Lett. **79**, 325 (1997).

[3] A. Ekert and R. Jozsa, quant-ph/9803072 (unpublished).

[4] R. Jozsa, quant-ph/9707034 (unpublished).

[5] V. Vedral and M. B. Plenio, quant-ph/9802065 (unpublished).

[6] C. H. Bennett, G. Brassard, and N. D. Mermin, Phys. Rev. Lett. **68**, 557 (1992).

[7] J. Kempe, Phys. Rev. A **60**, 910 (1999).

[8] C. H. Bennett *et al.*, Phys. Rev. Lett. **70**, 1895 (1993).

[9] C. H. Bennett *et al.*, Phys. Rev. Lett. **76**, 722 (1996).

[10] S. L. Braunstein, G. M. D'Ariano, G. J. Milburn, and M. F. Sacchi, quant-ph/9908036 (unpublished).

[11] M. B. Plenio and V. Vedral, quant-ph/9804075 (unpublished).

[12] S. L. Braunstein, C. A. Fuchs, and H. J. Kimble, quant-ph/9910030 (unpublished).

[13] S. L. Braunstein and H. J. Kimble, Phys. Rev. Lett. **80**, 869 (1998).

[14] S. L. Braunstein and H. J. Kimble, quant-ph/9910010 (unpublished).

[15] C. H. Bennett, P. W. Shor, J. A. Smolin, and A. V. Thapliyal, Phys. Rev. Lett. **83**, 3081 (1999).

[16] B. Schumacher, Phys. Rev. A **54**, 2614 (1996).

[17] B. Schumacher and M. A. Nielsen, Phys. Rev. A **54**, 2629 (1996).

[18] S. Hill and W. K. Wootters, Phys. Rev. Lett. **78**, 5022 (1997).

[19] C. H. Bennett, D. P. DiVincenzo, J. A. Smolin, and W. K. Wootters, Phys. Rev. A **54**, 3824 (1996).

[20] W. K. Wootters, quant-ph/9709029 (unpublished).

[21] D. P. DiVincenzo *et al.*, quant-ph/9803033 (unpublished).

[22] V. Vedral, M. B. Plenio, M. A. Rippin, and P. L. Knight, Phys. Rev. Lett. **78**, 2275 (1997).

[23] V. Vedral and M. B. Plenio, Phys. Rev. A **57**, 1619 (1998).

[24] D. Jonathan and M. B. Plenio, Phys. Rev. Lett. **83**, 3566 (1999).

[25] D. Jonathan and M. B. Plenio, Phys. Rev. Lett. **83**, 1455 (1999).

[26] P. Horodecki, M. Horodecki, and R. Horodecki, Phys. Rev. Lett. **82**, 1056 (1999).

[27] V. Bužek *et al.*, Phys. Rev. A **55**, 3327 (1997).

[28] W. Dür and J. I. Cirac, quant-ph/0002028 (unpublished).

[29] M. Murao, M. B. Plenio, and V. Vedral, Phys. Rev. A **61**, (2000).

[30] V. Vedral, quant-ph/9908047 (unpublished).

[31] A. Furusawa, J. L. Sørensen, S. L. Braunstein, C. A. Fuchs, H. J. Kimble and E. S. Polzik, Science, **282**, 706 (1998).

[32] D. Boschi *et al.*, Phys. Rev. Lett. **80**, 1121 (1998).

[33] G. J. Milburn and S. L. Braunstein, Phys. Rev. A **60**, 937 (1999).

[34] P. Rungta *et al.*, quant-ph/0001075 (unpublished).

[35] P. Deuar, W. J. Munro, and K. Nemoto, quant-ph/0002002 (unpublished).

[36] A. O. Pittenger and M. H. Rubin, quant-ph/0001110 (unpublished).

[37] W. Dür, J. I. Cirac, M. Lewenstein, and D. Bruß, quant-ph/9910022 (unpublished).

[38] O. Rudolph, quant-ph/0002026 (unpublished).

[39] P. Horodecki, quant-ph/9703004 (unpublished).

[40] A. Peres, Phys. Rev. Lett. **77**, 1413 (1996).

[41] M. Raymer, M. Beck and D. McAllister, Phys. Rev. Lett. **72**, 1137 (1994); R. Laflamme, E. Knill, W. H. Zurek, P. Catasti and S. V. S. Mariappan, Phil Trans. R. Soc. Lond. A **356**, 1941 (1998).

[42] C. H. Bennett, D. P. DiVincenzo, J. A. Smolin, W. K. Wootters, Phys. Rev. A **54**, 3824 (1996).

[43] A. Wherl, Rev. Mod. Phys. **50**, 221 (1978).

[44] A. Imamoglu and Y. Yamamoto, Phys. Rev. Lett. **72**, 210 (1994); C. L. Foden, V. I. Talyanskii, G. J. Milburn, M. L. Leadbeater and M. Pepper, to appear Phys. Rev B (2000); B. Lounis and W. E. Moerner, Nature ?????? (2000).

[45] M. Nielsen and I. Chuang, *Quantum Computation and Quantum Information*, (Cambridge University Press, Cambridge 2000).

[46] C. M. Caves and G. J. Milburn, quant-ph/9910001 (unpublished).

[47] D. F. Walls and G. J. Milburn, *Quantum Optics* (Springer-Verlag, Berlin, 1995).

[48] L. Susskind and J. Glogower, Physics **1**, 49 (1964).

[49] S. L. Braunstein, C. M. Caves, and G. J. Milburn, Annals of Physics **247**, 135 (1996).

[50] H. M. Wiseman, Ph.D. thesis, The University of Queensland, 1994.

[51] B. C. Sanders and G. J. Milburn, Phys. Rev. Lett. **75**, 2944 (1995).

[52] P. T. Cochrane, G. J. Milburn, and W. J. Munro, Phys. Rev. A **59**, 2631 (1999).

[53] L. C. Biedenharn and J. D. Louck, *Angular Momentum in Quantum Physics—Theory and Application* (Addison-Wesley, Reading, MA, 1981).

APPENDIX A: OPERATORS

1. Number projectors

We construct the number sum projector from consideration of the total number state

$$\rho = \sum_{n,m=0}^{\infty} |n\rangle_{A\otimes} \langle n| |m\rangle_B \langle m| \quad (A1)$$

The action of the number sum operator on this state gives

$$\hat{N}_+ \rho = \sum_{n,m=0}^{\infty} (n+m) |n\rangle \langle n| \otimes |m\rangle \langle m| \quad (A2)$$

letting $n = \frac{k+l}{2}$ and $m = \frac{k-l}{2}$ we find that after measurement of the number sum k the conditional state Eq. (A2) becomes

$$\begin{aligned} \rho^{(k)} = & \sum_{k=0}^{\infty} k \\ & \times \sum_{l=-k}^k \left| \frac{k+l}{2} \right\rangle \left\langle \frac{k+l}{2} \right| \otimes \left| \frac{k-l}{2} \right\rangle \left\langle \frac{k-l}{2} \right| \quad (A3) \end{aligned}$$

letting $2n = l + k$ gives

$$\rho^{(k)} \sum_{k=0}^{\infty} k \sum_{n=0}^k |n\rangle \langle n| \otimes |k-n\rangle \langle k-n|. \quad (\text{A4})$$

So, after a trivial change of variables, for the number sum measurement result q the projector is

$$\mathcal{N}_+ = \sum_{p=0}^q |q-p\rangle \langle p| \otimes |p\rangle \langle q-p|. \quad (\text{A5})$$

To find the number difference projectors we follow a similar procedure to above; acting the number difference operator on the state Eq. (A1) gives

$$\hat{N}_- \rho = \sum_{n,m=0}^{\infty} (n-m) |n\rangle \langle n| \otimes |m\rangle \langle m|. \quad (\text{A6})$$

Letting $n - m = k$ and $n + m = l$ we find that the state conditional on the measurement result k is

$$\begin{aligned} \rho^{(k)} &= \sum_{k=-\infty}^{\infty} k \\ &\times \sum_{l=|k|}^{\infty} \left| \frac{l+k}{2} \right\rangle \left\langle \frac{l+k}{2} \right| \otimes \left| \frac{l-k}{2} \right\rangle \left\langle \frac{l-k}{2} \right| \end{aligned} \quad (\text{A7})$$

We will arrive at two number difference projectors, one corresponding to a positive number difference result and one to a negative number difference result. Choosing $k \geq 0$ will give us the positive number difference result and simplifies Eq. (A7) to

$$\begin{aligned} \rho^{(k)} &= \sum_{k=0}^{\infty} k \\ &\times \sum_{l=k}^{\infty} \left| \frac{l+k}{2} \right\rangle \left\langle \frac{l+k}{2} \right| \otimes \left| \frac{l-k}{2} \right\rangle \left\langle \frac{l-k}{2} \right|, \end{aligned} \quad (\text{A8})$$

letting $2n = l - k$ gives the conditional state as

$$\rho^{(k)} = \sum_{k=0}^{\infty} k \sum_{n=0}^{\infty} |n+k\rangle \langle n+k| \otimes |n\rangle \langle n|. \quad (\text{A9})$$

Making a change of variables gives the number difference projector for the positive number difference result q ,

$$\mathcal{N}_-^{(+)} = \sum_{p=0}^{\infty} |p+q\rangle \langle p+q| \otimes |p\rangle \langle p|, \quad (\text{A10})$$

To find the projector for a negative number difference result we choose $k < 0$ and set $k' = -k$ in Eq. (A7) which simplifies to

$$\begin{aligned} \rho^{(k')} &= \sum_{k'=0}^{\infty} k' \\ &\times \sum_{l=k'}^{\infty} \left| \frac{l-k'}{2} \right\rangle \left\langle \frac{l-k'}{2} \right| \otimes \left| \frac{l+k'}{2} \right\rangle \left\langle \frac{l+k'}{2} \right| \end{aligned} \quad (\text{A11})$$

Letting $2n = l - k$ simplifies this to

$$\rho^{(k')} = \sum_{k'=0}^{\infty} k' \sum_{n=0}^{\infty} |n\rangle \langle n| \otimes |n+k'\rangle \langle n+k'|, \quad (\text{A12})$$

so, after a change of variables, the projector for a negative number difference measurement $q' = -q$ is

$$\mathcal{N}_-^{(-)} = \sum_{p=0}^{\infty} |p\rangle \langle p| \otimes |p+q'\rangle \langle p+q'| \quad (\text{A13})$$

2. Phase projectors

The phase difference and the phase sum projection operators are derived by integrating the total phase operator over the relevant variable.

The total phase operator is

$$\begin{aligned} |\phi_1\rangle \langle \phi_1| \otimes |\phi_2\rangle \langle \phi_2| &= \\ \sum_{w,x,y,z=0}^{\infty} e^{i[(w-x+y-z)\phi_+ + (x-w+y-z)\phi_-]} \\ \times |w\rangle \langle x| \otimes |y\rangle \langle z|. \end{aligned} \quad (\text{A14})$$

The phase difference projector is obtained by integrating Eq. (A14) over ϕ_+ in the region $[0, 2\pi]$,

$$\begin{aligned} |\phi_-\rangle \langle \phi_-| &= \sum_{w,x,y,z=0}^{\infty} e^{i(x-w+y-z)\phi_-} \delta_{w-x,z-y} \\ \times |w\rangle \langle x| \otimes |y\rangle \langle z|. \end{aligned} \quad (\text{A15})$$

and the phase sum projector is obtained similarly

$$\begin{aligned} |\phi_+\rangle \langle \phi_+| &= \sum_{w,x,y,z=0}^{\infty} e^{i(w-x+y-z)\phi_+} \delta_{x-w,z-y} \\ \times |w\rangle \langle x| \otimes |y\rangle \langle z|. \end{aligned} \quad (\text{A16})$$

APPENDIX B: ROTATION MATRIX COEFFICIENTS

The distribution of states in the resource is described by the rotation matrix coefficients defined by

$$d_{m',m}^j(\beta) = {}_z\langle j, m' | e^{-i\beta \hat{J}_x} | j, m \rangle_z. \quad (\text{B1})$$

It is easier to calculate these matrix elements using \hat{J}_y so we rotate about \hat{J}_z .

$$\begin{aligned}
& {}_z\langle j, m' | e^{-i\beta\hat{J}_x} | j, m \rangle_z \\
&= {}_z\langle j, m' | e^{-i\frac{\pi}{2}\hat{J}_z} e^{-i\beta\hat{J}_y} e^{i\frac{\pi}{2}\hat{J}_z} | j, m \rangle_z \\
&= {}_z\langle j, m' | e^{-i\frac{\pi}{2}m'} e^{-i\beta\hat{J}_y} e^{i\frac{\pi}{2}m} | j, m \rangle_z \\
&= e^{-i\frac{\pi}{2}(m'-m)} {}_z\langle j, m' | e^{-i\beta\hat{J}_y} | j, m \rangle_z \\
&= e^{-i\frac{\pi}{2}(m'-m)} D_{m',m}^j(\beta)
\end{aligned} \tag{B2}$$

where

$$D_{m',m}^j(\beta) = {}_z\langle j, m' | e^{-i\beta\hat{J}_y} | j, m \rangle_z, \tag{B3}$$

which are discussed in detail in [53]. These rotation matrix coefficients may be written in the more explicit form

$$\begin{aligned}
D_{m',m}^j(\beta) &= [(j+m')!(j-m')!(j+m)!(j-m)!]^{\frac{1}{2}} \\
&\times \sum_s \frac{(-1)^{m'-m+s} \left(\cos \frac{\beta}{2}\right)^{2j+m-m'-2s} \left(\sin \frac{\beta}{2}\right)^{m'-m+2s}}{(j+m-s)!s!(m'-m+s)!(j-m'-s)!}
\end{aligned} \tag{B4}$$

where s ranges over all integer values where the factorials are non-negative.

For equal photon number incident on each port of a 50:50 beam splitter we have $m = 0$, $j = N$ and $\beta = \frac{\pi}{2}$. The distribution of the coefficients defined in Eq. (B1) is shown in Figure 20.

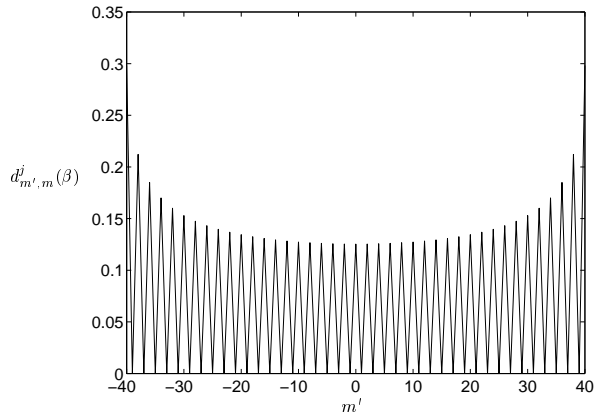


FIG. 20. Distribution of $d_{m',m}^j(\beta)$ coefficients for $j = 40$, $m = 0$ and $\beta = \frac{\pi}{2}$.

Note that every second term is zero, this is the reason why continuous target states will have a maximum fidelity of a half using the beam splitter generated resource.

One finds that as N increases the region in the middle of the distribution becomes flatter, thereby approaching the entanglement properties of the flat distribution $d_n = 1/\sqrt{N+1}$, discussed in Section III.